Redox Behavior and Dispersion of Supported Chromium Catalysts

Bert M. Weckhuysen,* Leo M. De Ridder, Piet J. Grobet, and Robert A. Schoonheydt

Centrum voor Oppervlaktechemie en Katalyse, K. U. Leuven, Kardinaal Mercierlaan 92, B-3001 Heverlee, Belgium

Received: June 30, 1994; In Final Form: September 19, 1994[⊗]

Supported chromium catalysts with different support composition are studied by electron spin resonance spectroscopy (ESR), thermogravimetrical analysis (TGA), and ^{27}Al magic angle spinning nuclear magnetic resonance (MAS-NMR). With ESR, the presence of Cr^{5+} (γ-signal) and two types of Cr^{3+} (δ- and β-signals) are observed; however, their concentrations are support-, loading-, and pretreatment-dependent. The Cr^{5+} loading increases with the alumina content of the support and can be maximized after moderate reduction temperatures and by using relatively low Cr loadings. Dispersed Cr^{3+} (δ-signal) is formed by reduction, and its amount increases with Al content of the support, Cr loading, and reduction temperature. On silica−alumina and alumina it is stable against recalcination. Cr_2O_3-like clusters (β-signal) are observed only on Cr/alumina after reduction and recalcination. TGA analysis indicates an increasing interaction strength between Cr and the support from silica over silica−alumina to alumina. The quenching of the ^{27}Al lines by paramagnetic Cr^{3+} was observed by ^{27}Al MAS-NMR measurements on the recalcined samples. This quenching effect was stronger on the Cr/alumina sample than on the Cr/silica−alumina samples, indicating Cr^{3+} substitution in octahedral Al sites. The observed differences in redox behavior and dispersion of Cr between the catalysts are discussed in terms of the support properties and in relation with previous results obtained by diffuse reflectance spectroscopy (DRS).

Introduction

Supported chromium catalysts are known to possess interesting catalytic properties.[1−5] The most important industrial application is in the production of polyethylene, known as the Phillips Particle Form Process.[6] These catalysts are usually activated by a high-temperature oxidative pretreatment, followed by reduction using ethylene or CO.[7] Our knowledge of these catalysts is—despite large efforts—largely qualitative: different oxidation states (Cr^{2+}, Cr^{3+}, Cr^{5+}, and Cr^{6+}) and different molecular structures (chromate, dichromate, etc.) have been identified with infrared spectroscopy[8] (IR), X-ray photoelectron spectroscopy[9] (XPS), Raman spectroscopy[10] (RS), diffuse reflectance spectroscopy[11] (DRS), and electron spin resonance[12] (ESR). However, if one ever wants to relate these species with catalytic performances, quantitative measurements are necessary.

Therefore, a research program has been set up for the development of methods to quantify Cr^{n+} species (with n between 2 and 6) and to elucidate the molecular structure of Cr in inorganic oxides. In previous studies,[13−15] we have reported (1) the quantification of Cr^{2+}, Cr^{3+}, and Cr^{6+} by diffuse reflectance spectroscopy (DRS) after calcination, reduction, and recalcination, (2) the elucidation of the molecular structure of Cr^{6+} by DRS, and (3) the interaction between different probe molecules and supported Cr. Under hydrated conditions, the molecular structure is determined by the pH at zero point of charge (zpc) of the support and by the Cr loading. At low Cr loading, the chromate:dichromate ratio increases with increasing alumina content of the support or pH at ZPC of the support. At higher loadings, Cr is more polymerized, even on an alumina support.[16] On calcined surfaces, the molecular structure is support and loading dependent. At relatively low Cr loadings, the dichromate:chromate ratio is highest for silica, zero for alumina, and in between for silica−aluminas. Upon reduction, octahedral Cr^{3+} and octahedral and tetrahedral Cr^{2+} are formed. The ratio tetrahedral:octahedral Cr^{2+} at constant loading and reduction temperature depends on the support and follows the order silica > silica−alumina > alumina. The ratio Cr^{2+}:Cr^{3+} increases with reduction temperature for all supports, but at the same reduction temperature, the ratio follows the sequence silica > silica−alumina > alumina.

Complementary results obtained by electron spin resonance (ESR), ^{27}Al magic angle spinning nuclear magnetic resonance (MAS-NMR), and thermogravimetrical analysis (TGA) are presented in this paper. The ESR spectra are quantified and related to the previously published quantitative DRS data. The link between silica and alumina is made through the investigation of a series of silica−aluminas with different silica contents. The results will be discussed in terms of redox behavior and dispersion of Cr. An overall picture of the relative concentrations of Cr^{2+}, Cr^{3+}, Cr^{5+}, and Cr^{6+} on amorphous supports after different pretreatments emerges.

Methods

1. Sample Preparation and Characterization. The preparation of SiO_2 (SA100) and SiO_2·Al_2O_3 with 20, 40, and 60 wt % SiO_2 (SA20, SA40, and SA60) and the characteristics of these supports are described elsewhere.[13,14] Two Al_2O_3 supports, one (SA0(I)) from Rhône-Poulenc and the other homemade (SA0-(HM)), were used. Their preparation and physical properties were published elsewhere.[13,14] The supported Cr catalysts were prepared by the incipient wetness technique with aqueous solutions of chromium(VI) trioxide (CrO_3). The chromium loadings were 0.1, 0.2, 0.4, 0.8, 1, 2, 4, and 8 wt % Cr. The impregnated samples were dried at 50 °C for 8 h and granulated. The selected size fraction was 0.25−0.40 mm.

2. Experimental Techniques. *2.1. Electron Spin Resonance Spectroscopy.* The granulated samples were loaded in a

* To whom correspondence should be addressed.

[⊗] Abstract published in *Advance ACS Abstracts,* December 1, 1994.

0022-3654/95/2099-0320$09.00/0

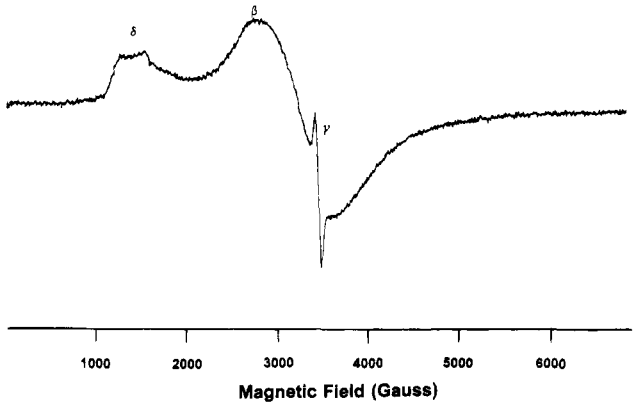

Figure 1. ESR spectrum of 0.8 wt % Cr/SA0(I) after recalcination at 550 °C (of the reduced sample) measured at 370 K (after oxygen evacuation): presence of γ-, β-, and δ-signals (the additional signal at $g = 4.3$ is due to Fe impurities of the support).

quartz flow cell with Suprasil window for diffuse reflectance spectroscopy (DRS) and a side arm for electron spin resonance spectroscopy (ESR). With this cell, it was possible to take DRS and ESR spectra after the same pretreatment. The DRS spectra were discussed in previous papers.[13-16] All the samples were calcined at 550 °C. The catalysts with a Cr loading between 0 and 0.8 wt % were subsequently reduced in a flow of CO at 200, 300, 400, and 600 °C during 0.5 h and recalcined at 550 °C. After each treatment ESR spectra were recorded between 120 and 370 K. The ESR spectra were taken using a Bruker ER 200 D-SRC instrument in X-band at a microwave power of 200 μW with a double rectangular TE_{104} mode cavity. Quantitative measurements were performed with a Bruker ESP 300E instrument in X band. Absolute spin concentrations were determined after double integration of the obtained spectra by using $Cu(acac)_2$/KCl (acac = acetylacetonate) mixtures as standards (number of spins: $10^{16}-10^{19}$/g).

2.2. Thermogravimetrical Analysis. Thermogravimetrical analyses were performed on powdered samples, typically 20–40 mg, using the TG-DTA 92 of Setaram. All samples were measured in a dynamic atmosphere of dry oxygen in helium. The supports, the Cr catalysts, and CrO_3 were dried at 100 °C calcination for 1 h, followed by calcining for 0.5 h at 550 °C (heating rate of 10 °C/min) *in situ* in the thermobalance.

2.3. ^{27}Al MAS-NMR Spectroscopy. ^{27}Al MAS-NMR measurements were performed using a Bruker MSL 400 spectrometer at 104.2 MHz in a magnetic field of 9.4 T, with a tipping angle of about 15° and a spinning frequency of 14.5 kHz. Approximately 2000 scans were accumulated. The spectra were deconvoluted into Gaussian bands, the individual bands were integrated, and the integrated areas were expressed per unit weight of dry catalysts.

2.4. X-ray Diffraction. X-ray diffraction patterns were recorded using an automated Siemens diffractometer, equipped with a Kristalloflex K710 röntgengenerator and a position-sensitive detector of Inel.

Results

1. Electron Spin Resonance of Supported Cr Catalysts.

1.1. Qualitative Electron Spin Resonance. Three signals can be present in the ESR spectra of Cr-supported catalysts, as illustrated in Figure 1 for Cr/Al_2O_3. These ESR signals are well described in the literature and usually denoted as γ, β, and δ.[7,17] The γ-signal is a sharp axially symmetric signal around $g = 1.9$, attributed to isolated, mononuclear Cr^{5+} species.[18] However, the hypothesis of a trimer of mixed valency ($Cr^{6+}-Cr^{3+}-Cr^{6+}$) with average oxidation state of 5 is also

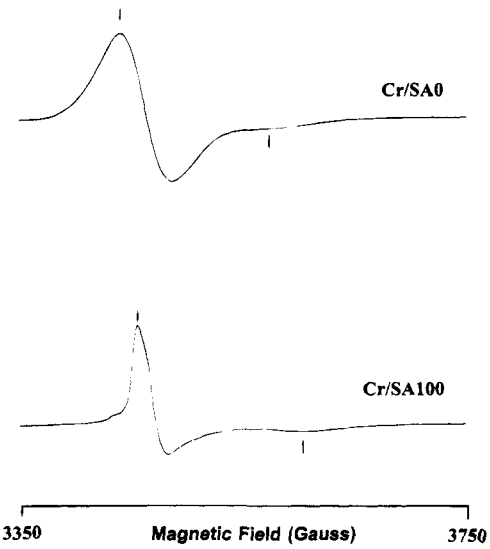

Figure 2. ESR spectra of the γ-signal of 0.2 wt % Cr/SA0(HM) (A) and Cr/SA100 after calcination at 550 °C measured at 120 K (after oxygen evacuation).

proposed in the literature.[19,20] This signal is formed on all supports. It attains its maximum intensity after reduction in the range 200–300 °C, the exact temperature depending on support and loading. Severe reduction pretreatments result in a total disappearance of this signal, while recalcination re-establishes it. The β-signal is ascribed to Cr_2O_3-like clusters and is only formed on alumina after reduction and recalcination. Its amount increases with increasing Cr loading. The δ-signal, usually assigned to magnetically isolated or dispersed Cr^{3+} species,[7,17,21] is formed on all supports after reduction. Its amount increases with increasing reduction temperature and Cr loading and remains in the spectra after recalcination on silica–alumina and alumina.

1.2. Characteristics of the γ-, β-, and δ-Signals. 1.2.1. γ-Signal. The shape of the γ-signal depends on the support as shown in Figure 2 for Cr/SA0(HM) and Cr/SA100. The γ-signals of the Cr/SAn catalysts with $n = 20$, 40, and 60 are similar to those of Cr/SA0, suggesting Cr^{5+} in Al-rich phases. The g values were obtained by simulation with an axially symmetric Hamiltonian. The signals are usually interpreted as due to axially symmetric $[CrO_4]^{3-}$ species with $g_\perp = 1.975-1.895$ and $g_{||} = 1.895$ and an axially distorted tetrahedral species with $g_\perp = 1.980$ and $g_{||} = 1.950$, the latter signal being resolved on SiO_2 only. The increase of the line width in going from silica to alumina is probably due to interaction of the unpaired electron of Cr^{5+} with the ^{27}Al nuclei ($I = 5/2$). In any case, all Cr^{5+} are surface species, because line broadening is observed in the presence of O_2 at room temperature.

The intensities of the γ-signal follow the Curie–Weiss law, independently of the pretreatment and Cr loading. As an example, the reciprocal of the ESR intensities is plotted as a function of temperature ($I^{-1}-T$ plots) for Cr/SA100 in Figure 3. It is clear that the plots are almost linear, after linear extrapolation, and intersect the abscissa at 100–110 K. This is in accordance with Curie–Weiss behavior[22]

$$\chi_{Cr^{5+}} = \frac{C}{T-\theta} \sim I_{Cr^{5+}} \qquad (1)$$

where C is the Curie constant, χ the molar susceptibility, T the absolute temperature, and θ the Weiss constant. θ depends on the support composition. For Cr/SA0 and Cr/SA40 θ is respectively around 35–45 and 0–10 K. The latter numbers are obtained by linear extrapolation from ESR intensity mea-

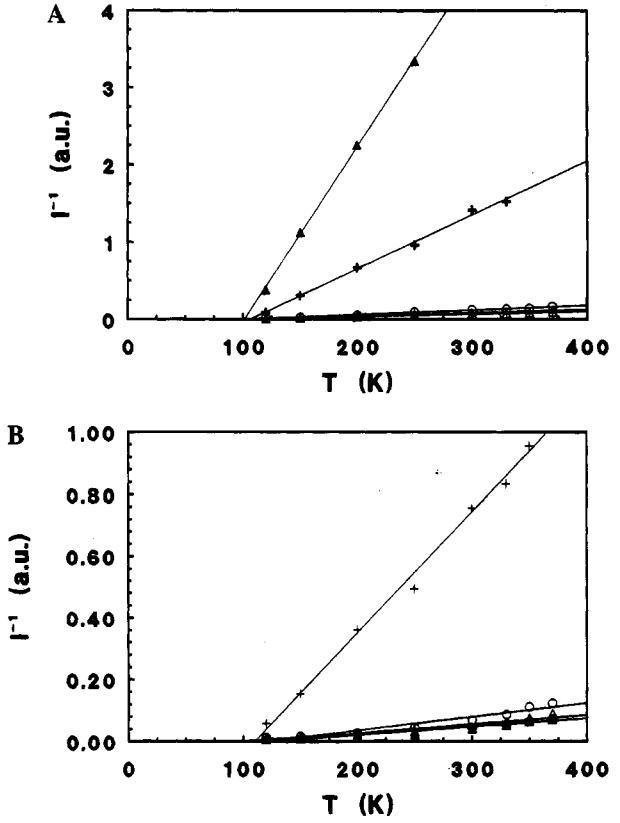

Figure 3. (A) Reciprocal ESR intensities of Cr^{5+} as a function of temperature of the Cr/SA100 catalyst (0.2 wt %) after different pretreatments: calcination at 550 °C (△); reduction at 200 (+), 300 (○), 400 (bold +), and 600 °C (▲). (B) Reciprocal ESR intensities of Cr^{5+} as a function of temperature of the Cr/SA100 catalyst for different Cr loadings: 0.2 (+), 1.0 (△), 2.0 (○), 4.0 (bold +), and 8.0 wt % (▲).

surements above 110 K. The validity of this extensive extrapolation was not verified. In any case, the data do show that the magnetic behavior of Cr^{5+} is strongly support dependent. The extent to which θ deviates from zero is a measure of the extent of $Cr^{5+}-Cr^{5+}$ interaction. Small θ values mean magnetically dilute Cr^{5+} systems, and high θ values mean magnetically concentrated Cr^{5+} systems. If this is taken as an indication of dispersion of Cr over the supports, then Cr dispersion increases in the order $SiO_2 \ll Al_2O_3 < SiO_2{\cdot}Al_2O_3$.

1.2.2. β-Signal. In our experiments, the β-signal is only visible after reduction and recalcination of Cr/Al_2O_3 and can be easily studied after strong reduction and recalcination. The dependence of the β-signal on pretreatment is shown in Figure 4. It is observed that the β-signal is broad and weak during the first reduction cycle. The peak-to-peak line widths (ppw) are in the range 1200−2000 G, while the g values are around 2.45−2.09. Both parameters have a tendency to decrease with increasing reduction temperature. The signal becomes pronounced after recalcination with $g = 2.2$ and a ppw of 900 G. Furthermore, the ppw decreases with increasing Cr loading.

Above 320 K, the β-signal follows the Curie−Weiss law, but its thermal behavior changes in the region 280−310 K, while lower temperatures broaden the signal. The Néel temperature (T_N) of α-Cr_2O_3 is around 307 K,[23] close to the 320 K, the limiting temperature for Curie−Weiss behavior of our samples. This indicates that the β-signal on alumina is due to Cr_2O_3-like clusters, which are, however, too small in size or too small in number to be detected by XRD. The decrease of the ppw and the g value with reduction temperature suggests growing cluster sizes, the line shape being determined by exchange coupling and dipolar interaction between the Cr^{3+} ions. The first results

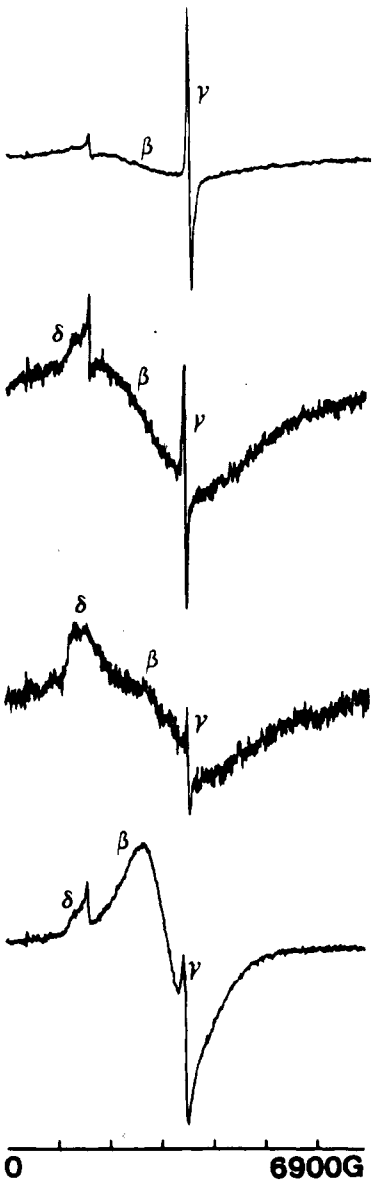

Figure 4. β-signal as a function of pretreatment for 0.2 wt % Cr/SAO(I): A, reduction at 300 °C; B, reduction at 400 °C; C, reduction at 600 °C; D, recalcination at 550 °C.

in an exchange narrowing of the resonance line; the second phenomenon gives line broadening.[17] Therefore, smaller ppw's suggest larger Cr_2O_3-like clusters. Our results indicate that these clusters grow in size by increasing the reduction temperature, by increasing the Cr loading, and especially by recalcination. It is remarkable that no β-signal is observed on $Cr/SiO_2{\cdot}Al_2O_3$ clusters and on Cr/SiO_2, but it does not mean that Cr_2O_3-like clusters are absent. The β-signals on these supports may be broadened beyond detection.

1.2.3. δ-Signal. The δ-signal of dispersed Cr^{3+} ions appears on all the supports after reduction (Figure 5). The intensity of this signal increases with increasing Cr loading and reduction temperature. For the same reduction temperature it increases with the alumina content of the support. The position of the signal is also a function of the support: the maximum of the δ-signal is at higher fields for Cr/SA100 (g around 4.4) than for the other supports (g around 5.0−5.5). After recalcination the signal is absent in the Cr/SA100 samples but remains on the other supports. This suggests that isolated Cr^{3+} ions are stabilized in or on Al_2O_3 and $SiO_2{\cdot}Al_2O_3$ in such a way that they resist oxidation.

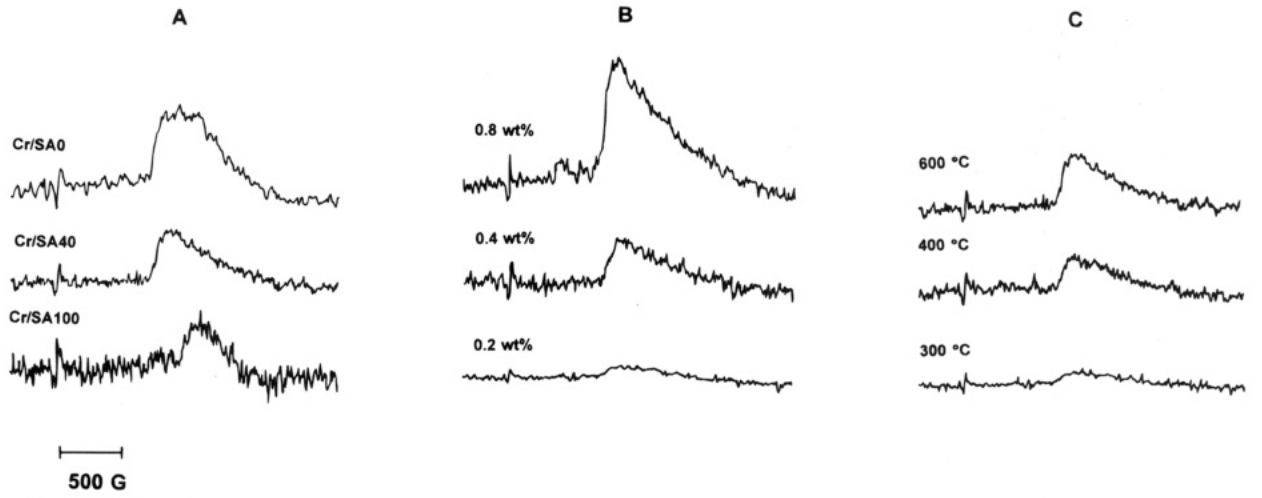

Figure 5. δ-signal as a function of support type (A, 0.4 wt % after reduction at 600 °C), as a function of Cr loading (B, Cr/SA40 after reduction at 600 °C), and as a function of pretreatment (C, Cr/SA60, 0.4 wt %).

1.3. Quantitative Electron Spin Resonance. Quantitative determination of Cr^{5+} and Cr^{3+} species is possible by comparison with a reference sample with known spin density, according to formula 2:

$$N_{Cr^{n+}} = N_{REF} \frac{A_{Cr^{n+}}}{A_{REF}} \frac{g_{REF}}{g_{Cr^{n+}}} \frac{S_{REF}(S_{REF}+1)}{S_{Cr^{n+}}(S_{Cr^{n+}}+1)} \qquad (2)$$

where $N_{Cr^{n+}}$ and N_{REF} are the amount of spins of respectively Cr^{n+} and reference sample; $A_{Cr^{n+}}$ and A_{REF} are the integrated intensity of the ESR signal of respectively Cr^{n+} and reference sample; $g_{Cr^{n+}}$ and g_{REF} are the g value of respectively Cr^{n+} and reference sample; and $S_{Cr^{n+}}$ and S_{REF} are the spin quantum number of respectively Cr^{n+} and reference sample.

The reference is KCl diluted $Cu(acac)_2$ ($Cu^{2+} = d^9$) with $S_{REF} = {}^1/_2$ and $g_{REF} = 2.10$. For the γ-signal $S_{Cr^{5+}}$ is equal to ${}^1/_2$ and $g_{Cr^{5+}} = (2g_\perp + g_{||})/3$, while for the β- and δ-signal $S_{Cr^{3+}}$ is ${}^3/_2$. The integrated areas of the different signals were obtained as follows. The γ-signal was doubly integrated over a field of 500 G centered around $g = 1.9$ after a linear base line correction. If the β-signal was superposed on the γ-signal, a cubic base line correction was performed. The situation for the δ-signal is more complicated, because it is weak and its negative lobe probably extends to higher fields over a large field range. A rough estimate can be made by taking the area under the signal by single integration over a field of 3000 G centered around the maximum peak (after a linear base line correction). The area of the β-signal was obtained by double integration of both the β- and γ-signal and subtraction of the intensity of the γ-signal.

The amount of Cr^{5+} is always low (<2% of total Cr content), increases with increasing alumina content of the support, and reaches a maximum after reduction in the range 200−300 °C. The maximum is closer to 200 °C for SiO_2 and SiO_2·Al_2O_3 and to 300 °C for Al_2O_3 (Figure 6). After reduction at 600 °C the signal has almost completely disappeared. It reappears after recalcination. When studied as a function of loading, the relative Cr^{5+} concentration is maximum at low Cr loadings (0.4 wt % for Cr/SA0, 0.2 wt % for Cr/SA40, and 1.0 wt % for Cr/SA100) and decreases with increasing Cr loading. Summarizing, the Cr^{5+} concentration can be maximized with a high aluminum content of the support, moderate reduction temperatures with CO, and relatively low Cr loadings.

The amount of dispersed Cr^{3+} (δ-phase) increases with increasing alumina content and reduction temperature but is very low in all cases (< 0.4% of the total Cr content) and can only be roughly quantified. Our attempts to quantify the β-signal failed.

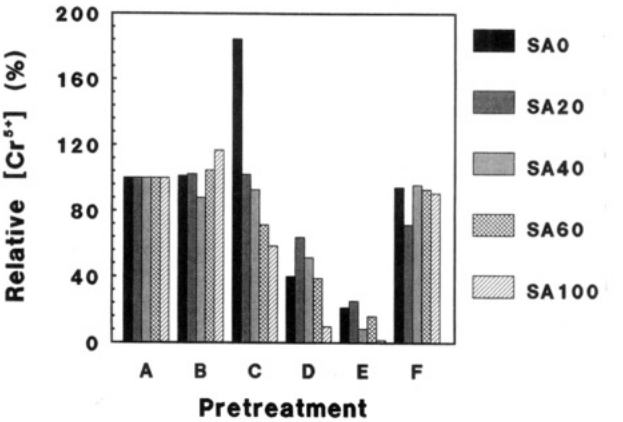

Figure 6. Relative amount of Cr^{5+} as a function of the support type and pretreatment (A, calcination; B, C, D, E, reduction at respectively 200, 300, 400, and 600 °C; F, recalcination) for 0.2 wt % supported Cr catalysts.

From the total Cr content determined by chemical analysis (Cr_{tot}), the amounts of Cr^{6+} and Cr^{3+} determined by DRS,[13] and the amount of Cr^{5+} determined by EPR, one obtains

$$[Cr^{2+}] = [Cr_{tot}] - ([Cr^{6+}] + [Cr^{3+}] + [Cr^{5+}]) \qquad (3)$$

This equation is valid up to 0.4 wt % for Cr/Al_2O_3, 0.2 wt % for Cr/SiO_2·Al_2O_3, and 0.1 wt % for Cr/SiO_2. These limits are dictated by the quantitative DRS data.[13] The amount of every Cr^{n+} species can now be plotted at different pretreatments as shown for Al_2O_3 in Figure 7. This figure is a refinement of our earlier published figure[13] in that $[Cr^{5+}]$ is incorporated. The figures for Cr/SiO_2 and Cr/SiO_2·Al_2O_3 are identical to the previously published figures, because $[Cr^{5+}]$ is too small to be shown.

For the calcined samples the amount of Cr^{5+} decreases sharply with the $[SiO_2]$:$[Al_2O_3]$ ratio and increases linearly with the [chromate]:[dichromate] ratio as shown in Figure 8, at least at ratios ≤4. The chromate:dichromate ratio, obtained by DRS, is a measure of the dispersion of Cr, and therefore, $[Cr^{5+}]$ can also be used as a dispersion criterion.

2. Thermogravimetry of Supported Chromium Catalysts. This analysis focuses on modifications of the thermal behavior of the chromium precursor (CrO_3) as a result of interactions

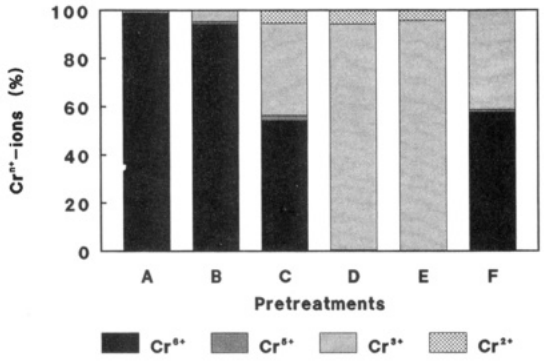

Figure 7. Distribution of Cr^{6+}, Cr^{5+}, Cr^{3+}, and Cr^{2+} on an 0.2 wt % Cr-loaded alumina surface as a function of pretreatment: calcination at 550 °C (A), reduction at 200 °C (B), reduction at 300 °C (C), reduction at 400 °C (D), reduction at 600 °C (E), and recalcination at 550 °C (F).

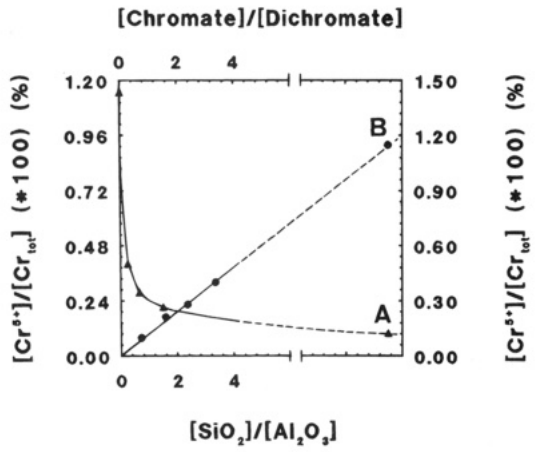

Figure 8. Amount of Cr^{5+} versus $[SiO_2]$:$[Al_2O_3]$ of the supports (A) and versus chromate:dichromate ratio (B) obtained by DRS.[13,14]

TABLE 1: α-Values of CrO_3-Impregnated SiO_2, Al_2O_3, and SiO_2·Al_2O_3 for Different Cr Loadings

Cr-loading (wt %)	$\alpha_{Cr/SA100}$	$\alpha_{Cr/SA40}$	$\alpha_{Cr/SA0}$
0.1	2.2	9.6	12.2
0.2	0.7	9.7	14.2
0.4	1.3	10.4	15.4
0.8	2.5	14.6	16.5

with the amorphous supports. Therefore, the Cr catalysts, the related supports, and CrO_3 were thermogravimetrically analyzed. A proposed measure for the interaction strength is the parameter α,[24] defined as

$$\alpha = \frac{\%\ WL_s \times 100}{\%\ WL_{us}} \qquad (4)$$

Here WL_{us} is the weight loss of the unsupported chromium compound (=CrO_3); this weight loss is 29.3%, near the stoichiometric value of 24% for $CrO_3 \rightarrow \alpha$-Cr_2O_3. WL_s is the weight loss of the supported chromium compound; this is the weight loss of the Cr catalysts diminished with the weight loss of the support without Cr.

The α-values of the Cr catalysts, calculated according to eq 4, are shown in Table 1. It is seen that (1) α increases for every support with the Cr loading, except for Cr/SiO_2 (SA100), and (2) for the same loading α-values increase from SiO_2 (SA100) over SiO_2·Al_2O_3 (SA40) to Al_2O_3 (SA0).

The data of Table 1 can then be explained in terms of a schematic picture of Figure 9 for the chromate adsorption on

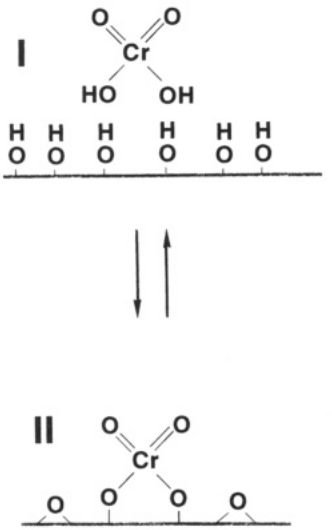

Figure 9. Interaction of chromate with alumina upon calcination: (I) before calcination and (II) after calcination (anchoraging of Cr with support dehydroxylation).

for example alumina. Case I is before anchoring (hydrated), while case II is after calcination (dehydrated). Thus, this figure shows the features upon calcination: dehydroxylation of the Cr catalyst is more extensive than that of the pure support because of the reaction of hydroxyls with Cr, and no or negligible clustering to Cr_2O_3 occurs (at least for low Cr loadings). In this case, α is positive, and the more Cr is anchored, the larger α.

Additional evidence for this mechanism comes from (1) our direct observation of consumption of OH groups upon Cr deposition by calcination[16] and (2) the small amounts of Cr_2O_3-like clusters detected by EPR in the present study and by DRS.[13,14] Then, the data of Table 1 show that the degree of interaction between Cr and the support increases from SiO_2 over SiO_2·Al_2O_3 to Al_2O_3 and the degree of interaction, expressed per mole of Cr, decreases with increasing Cr loading, except for Cr/SiO_2. The low α values of Cr/SiO_2 are explained by the presence of some dichromate, which releases only one H_2O per Cr upon chemisorption and by the presence of some Cr^{3+}.[13,14]

3. ^{27}Al MAS Nuclear Magnetic Resonance of Supported Chromium Catalysts. The ^{27}Al MAS-NMR spectra of the calcined samples are identical to those of the pure supports, while the spectra of the recalcined Cr/Al_2O_3 and Cr/SiO_2·Al_2O_3 are shown in Figure 10. The ^{27}Al spectra of Cr/Al_2O_3 show resonances around 55 and 0 ppm which are indicative of tetrahedral and octahedral coordination of Al, respectively.[25] The ^{27}Al spectra of Cr/SiO_2·Al_2O_3 show an extra resonance line around 30 ppm which is tentatively assigned to pentacoordinated Al.[26] Table 2 summarizes the intensities of the ^{27}Al MAS NMR lines after deconvolution in a tetrahedral peak, an octahedral peak, and a peak of pentacoordinated Al^{3+}. The octahedral peak of Cr/SiO_2·Al_2O_3 is asymmetric due to quadrupolar interaction. For Cr/Al_2O_3 the overall intensity decreases with increasing Cr loading, and this is the most pronounced for the octahedral line. For Cr/SiO_2·Al_2O_3 the intensities are independent of the Cr loading. It is known from the literature that paramagnetic species, like Cr^{n+} with $n < 6$, quench ^{27}Al lines in NMR[27,28] due to relaxation phenomena.[29] The data show that only octahedral Al^{3+} of Al_2O_3 is affected, suggesting that part of $Cr^{3+}(d^3)$ and $Cr^{5+}(d^1)$ occupies sites on/in Al_2O_3 in close vicinity of octhahedral ^{27}Al. This, apparently, is not the case for Cr/SiO_2·Al_2O_3.

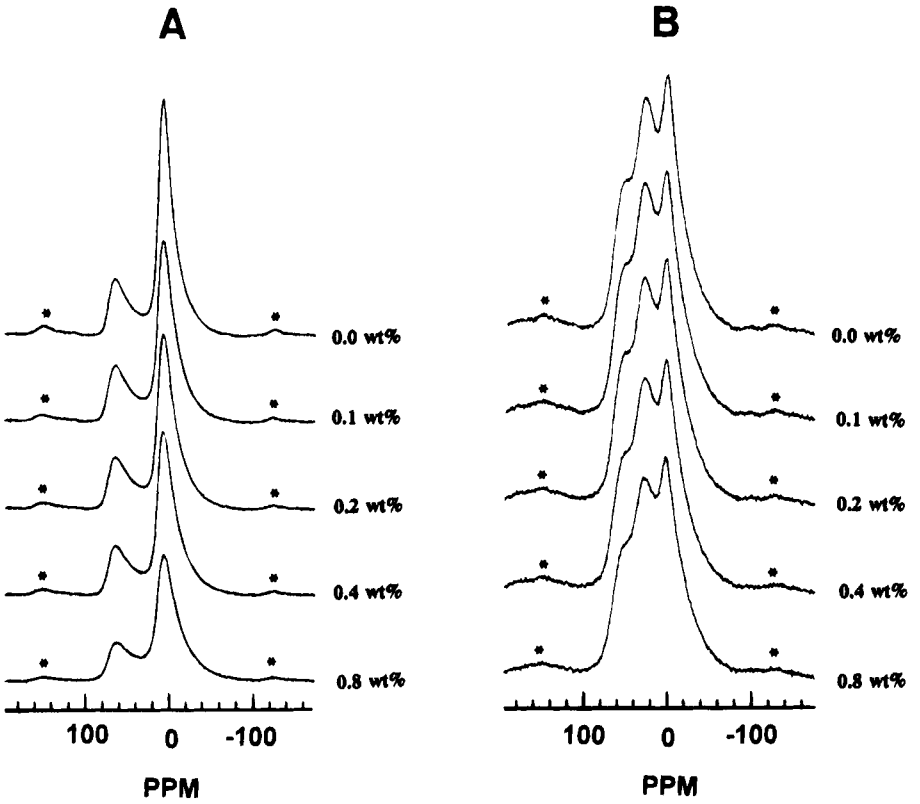

Figure 10. ^{27}Al MAS NMR spectra of recalcined Cr/Al_2O_3 (A) and $Cr/SiO_2{\cdot}Al_2O_3$ (B) for increasing Cr loading.

TABLE 2: ^{27}Al MAS NMR Results of Chromium Supported Catalysts after Recalcination (after a Successive Reduction Pretreatment)

Cr loading (wt%)	Cr/Al_2O_3 (SA0(I))[b]			$Cr/SiO_2{\cdot}Al_2O_3$ (SA40)[c]			
	IA_{tetr}[a]	IA_{oct}[a]	IA_{tot}[a]	IA_{tetr}[a]	IA_{penta}[a]	IA_{oct}[a]	IA_{tot}[a]
0.0	65	231	296	55	111	161	327
0.1	72	218	290	55	113	165	333
0.2	69	214	283	54	111	167	332
0.4	67	210	277	50	110	172	332
0.8	56	185	241	50	109	172	331

[a] IA_{tetr}, integrated area of tetrahedral peak; IA_{oct}, integrated area of octahedral peak; IA_{penta}, integrated area of pentahedral peak; IA_{tot}, integrated area of total spectrum. All the values were corrected for the water content of the samples. [b] Cr^{3+} loading (wt %) = 0.419 × Cr loading (wt %) (as determined by quantitative DRS).[13] [c] Cr^{3+} loading (wt %) = 0.632 × Cr loading (wt %) (as determined by quantitative DRS).[13]

Discussion

The data reported here, combined with our previously published DRS results,[13-15] allow the development of a quite general picture of the chemistry of Cr on oxides.

Three species, Cr^{5+}, Cr^{3+}, and Cr_2O_3-like clusters, are detected with EPR on supported Cr catalysts as γ-, δ-, and β-signals, respectively. The shape, the g values, and intensities of these signals reflect the type of support and the Cr loading. The Cr^{5+} and Cr^{3+} signal intensities are proportional to the Al_2O_3 content of the supports but correspond to no more than 2% of the total Cr content. Strong chromate adsorption sites, which prohibit Cr migration over the surface, are thought to be responsible for the generation of these Cr^{5+} and Cr^{3+} species, but some migration in the surface layers cannot be ruled out. In any case, the close proximity of Al is evident from (1) the broadening of the Cr^{5+} lines on Al_2O_3 with respect to SiO_2, (2) the difference in position of the Cr^{3+} lines on Al_2O_3 with respect to SiO_2, and (3) the decrease of the ^{27}Al NMR line intensity with Cr loading. It is also remarkable that the EPR signals of Cr^{5+} and Cr^{3+} on $SiO_2{\cdot}Al_2O_3$ resemble those of Al_2O_3, suggesting that these ions are preferentially located in the "Al_2O_3" parts of silica–aluminas.

If these γ- and δ-signals are due to atomically dispersed Cr^{5+} and Cr^{3+}, their intensities can be used as a dispersion criterion. This was confirmed by the linear relationship between the Cr^{5+} signal intensity and the chromate:dichromate ratio determined by DRS.[13,14] The latter is also an indication of dispersion. The Cr^{3+} signal is too broad to quantify properly, and its intensity cannot be used as dispersion criterion, although it follows the same trend as the Cr^{5+} signal. The same is valid for the Curie–Weiss constant of Cr^{5+} and its dependence on the type of support. Here, the θ values of Al_2O_3 and $SiO_2{\cdot}Al_2O_3$ are too uncertain. They do suggest, however, that dispersion is the lowest on SiO_2. The other dispersion criterion of this paper is the α-value. The larger α, the stronger the chromate anchoring and the better the dispersion. The trend is then alumina > silica–alumina ≫ silica, with silica–alumina closer to alumina than to silica. Thus, several criteria can be used to measure dispersion qualitatively. These criteria can be used in the whole Cr loading range: the higher the Cr loading, the lower Cr dispersion and the lower the α-values and $[Cr^{5+}]$. However, the Curie–Weiss constant of Cr^{5+} is only function of the support type and only easy measurable for low Cr loadings.

In summary, the proposed dispersion criteria all point toward the same trend: dispersion is the highest on Al_2O_3 and the lowest on SiO_2, with $SiO_2{\cdot}Al_2O_3$ in between. If they are Al-rich, chromium preferentially interacts with the "Al_2O_3" parts of silica–aluminas.

This support dependency of Cr dispersion can be explained by the amount and characteristics of the hydroxyl groups of the supports. It is known that the amount of hydroxyls increases with increasing Al content of the support. The more OH groups available for anchoring Cr, the better Cr will be dispersed. Furthermore, alumina surfaces possess more basic OH groups,

which will react more readily with the acid CrO_3 resulting in a better dispersion.

If dispersion of Cr is as indicated, then the amount and/or size of Cr_2O_3-like clusters should follow the reverse order: SiO_2 > SiO_2·Al_2O_3 > Al_2O_3. This cannot be seen from the β-signal in EPR. The intensity of the d−d transition in the range 15 000−18 000 cm^{-1} of Cr^{3+} in DRS behaves, however, as expected. Cr^{3+} is always seen on SiO_2 after calcination due to the reaction $2CrO_3 \rightarrow Cr_2O_3 + {}^3/_2O_2$. Such a reaction is also deduced from the α-values (Table 1). Therefore, Cr_2O_3-like clusters are formed on SiO_2 already after calcination. As a consequence, the dispersion is less on silica than on the other supports. The nearly total absence of a β-signal on silica in EPR must then be attributed to line broadening beyond detection. Why this is so on silica and not an alumina requires a detailed investigation of the β-signal dependence on the amount, size, and shape of Cr_2O_3 clusters.

Finally, the relation between dispersion of Cr and reduction to Cr^{2+} must be investigated. Cr^{2+} is only found in significant amounts on silica, and thus, there is a support and dispersion dependence. First of all, the interaction of Cr species is stronger with Al_2O_3 and SiO_2·Al_2O_3 than with SiO_2. The reason is the closeness of the ionic radii of Cr^{6+} (0.52 Å) and Cr^{3+} ($R(Cr^{3+}_{Oh})$ = 0.62 Å) with that of Al^{3+} ($R(Al^{3+}_{Oh})$ = 0.53 Å)[30] and the structural similarity between γ-Al_2O_3 (a spinel-like structure in which octahedral and tetrahedral aluminum ions are randomly distributed and which is formed by cubic close-packed oxygens[31]) and α-Cr_2O_3 (a structure built up with close-packed oxygens in a hexagonal arrangement[32]). This similarity can lead to an epitaxial growth of Cr_2O_3 clusters on the γ-Al_2O_3 surface, and therefore, it will be more difficult to reduce Cr^{3+} to Cr^{2+} on alumina than on silica. Finally, if aqueous solution standard reduction potentials are valid, then dichromate species are more easier reducible than chromate (to Cr^{3+}).[33] The former are present in significant amounts on SiO_2, and therefore, one expects the initial reducibility to follow the order SiO_2 > SiO_2·Al_2O_3 > Al_2O_3.

In summary, with X-band ESR spectroscopy $Cr^{5+}(d^1)$ and two types of $Cr^{3+}(d^3)$ (dispersed Cr^{3+} and Cr_2O_3-like clusters) are measured. DRS spectroscopy probes the charge transfers of $Cr^{6+}(d^0)$ in chromate and dichromate or polychromates and the d−d transitions of $Cr^{2+}(d^4)$ and $Cr^{3+}(d^3)$. Thus, DRS and ESR are complementary spectroscopic techniques with Cr^{3+} accessible by both techniques. In principle, $Cr^{5+}(d^1)$ could also be detected by DRS, but less than 2% of the total Cr content being Cr^{5+} is too small for detection. DRS is unable to differentiate between atomically dispersed Cr^{3+} and Cr_2O_3-like clusters, as is possible by ESR. Also, the amounts of Cr^{3+} measured with both techniques are not comparable. This suggests that only a small amount of Cr^{3+} is ESR-active. This speciation of the different oxidation states of Cr has recently been successfully extended to Cr molecular sieves.[34−36]

Conclusions

Cr^{5+}, Cr^{3+}, and Cr_2O_3-like clusters are the species detected on Cr-supported catalysts. The amounts of Cr^{5+} and Cr^{3+} increase from silica over silica−alumina to alumina but never exceed 2% of the total Cr content. Several qualitative dispersion criteria have been established: Cr^{5+} content, Curie−Weiss constant of Cr^{5+}, and α-parameter. They all indicate that the dispersion is lowest on silica and highest on alumina with silica−alumina in between, but closer to alumina than on silica. This indicates that Cr^{n+} preferentially interacts with the Al_2O_3 parts of silica−alumina. DRS and ESR are complementary techniques for speciation of Cr oxidation states on inorganic surfaces.

Acknowledgment. B.M.W. acknowledges the N.F.W.O. (Nationaal Fonds voor Wetenschappelijk Onderzoek) for a grant as research assistant. The authors thank Hilde Geerts for the ^{27}Al MAS-NMR measurements. This work is supported by the Fonds voor Kollectief Fundamenteel Onderzoek (FKFO) under Grant 2.0050.93.

References and Notes

(1) Zielinski, P. A.; Szymura, J. A.; Dalla Lana, I. G. *Catal. Lett.* **1992**, *13*, 331.
(2) Vuurman, M. A.; Wachs, I. E. *J. Phys. Chem.* **1992**, *96*, 5008.
(3) Cimino, A.; Cordischi, D.; De Rossi, S.; Ferraris, G.; Gazzoli, D.; Indovina, V.; Minelli, G.; Occhiuzzi, M.; Valigi, M. *J. Catal.* **1991**, *127*, 77.
(4) Charcosset, H.; Revillon, A.; Guyot, A. *J. Catal.* **1967**, *8*, 334.
(5) Hogan, J. P.; Banks, R. L. Belg. Pat. 530617, 1955.
(6) Hogan, J. P.; Norwood, D. D.; Ayres, C. A. *J. Appl. Polym. Sci.* **1981**, *36*, 49.
(7) McDaniel, M. P. *Adv. Catal.* **1985**, *33*, 47.
(8) Ghiotti, G.; Garrone, E.; Zecchina, A. *J. Mol. Catal.* **1988**, *46*, 61. Kim, C. S.; Woo, S. I. *J. Mol. Catal.* **1992**, *73*, 249.
(9) Best, S. A.; Squires, R. G.; Walton, R. A. *J. Catal.* **1977**, *47*, 292. Merryfield, R.; McDaniel, M.; Parks, G. *J. Catal.* **1982**, *77*, 348.
(10) Vuurman, M. A.; Stufkens, D. J.; Oskam, A.; Moulijn, J. A.; Kapteijn, F. *J. Mol. Catal.* **1990**, *60*, 83. Kim, D. S.; Tatibouet, J. M.; Wachs, I. E. *J. Catal.* **1992**, *136*, 209. Hardcastle, F. D.; Wachs, I. E. *J. Mol. Catal.* **1988**, *46*, 173. Deo, G.; Wachs, I. E. *J. Phys. Chem.* **1991**, *95*, 5889. Vuurman, M. A.; Hardcastle, F. D.; Wachs, I. E. *J. Mol. Catal.* **1993**, *84*, 193.
(11) Przhevalskaya, L. K.; Shvets, V. A.; Kazanskii, V. B. *Kinet. Katal.* **1970**, *11*, 1310. Zecchina, A.; Garrone, E.; Ghiotti, G.; Morterra, C.; Borello, E. *J. Phys. Chem.* **1975**, *79*, 966. Krauss, H. L.; Stach, H. *Z. Anorg. Allg. Chem.* **1969**, *366*, 34. Ghiotti, G.; Garrone, E.; Della Gatta, G.; Fubini, B.; Giamello, E. *J. Catal.* **1983**, *80*, 249.
(12) Köhler, K.; Shläpfer, C. W.; von Zelewsky, A.; Nickl, J.; Engweiler, J.; Baiker, A. *J. Catal.* **1993**, *143*, 201. Cordishi, D.; Indovina, V.; Occhiuzzi, M. *J. Chem. Soc., Faraday Trans.* **1991**, *87*, 3443.
(13) Weckhuysen, B. M.; De Ridder, L. M.; Schoonheydt, R. A. *J. Phys. Chem.* **1993**, *97*, 4756.
(14) Weckhuysen, B. M.; Verberckmoes, A. A.; Buttiens, A. L.; Schoonheydt, R. A. *J. Phys. Chem.* **1994**, *98*, 579.
(15) Weckhuysen, B. M.; Wachs, I. E.; Schoonheydt, R. A. *Stud. Surf. Sci. Catal.*, in press.
(16) Weckhuysen, B. M.; Schoonheydt, R. A.; Jehng, J. M.; Wachs, I. E. *J. Phys. Chem.*, submitted for publication.
(17) O'Reilly, D. E.; MacIver, D. S. *J. Phys. Chem.* **1962**, *66*, 276.
(18) Kazanski, V. B.; Turkevich, J. *J. Catal.* **1967**, *8*, 231.
(19) Spitz, R. *J. Catal.* **1974**, *35*, 345.
(20) Ellison, A. *J. Chem. Soc., Faraday Trans. 1* **1984**, *80*, 2581.
(21) Groeneveld, C.; Wittgen, P. P. M. M.; van Kersbergen, A. M.; Mestram, P. L. M.; Nuijten, C. E.; Schuit, G. C. A. *J. Catal.* **1979**, *59*, 153.
(22) Boudreaux, E. A.; Mulay, L. N. In *Theory and Applications of Molecular Paramagnetism*; Wiley: New York, 1979.
(23) Kittel, C. H. In *Introduction to Solid State Physics*, 3rd ed.; Wiley: New York, 1968.
(24) Fouad, N. E.; Knözinger, H.; Zaki, M. I.; Mansour, S. A. A. *Z. Phys. Chem.* **1991**, *171*, 75.
(25) Engelhardt, G.; Michel, D. In *High Resolution Solid State NMR of Silicates and Zeolites*; John Wiley & Sons: New York, 1982.
(26) Gilson, J. P.; Edwards, G. C.; Peters, A. W.; Rajagopalan, M. P. *J. Chem. Soc., Chem. Commun.* **1987**, 91.
(27) Bloembergen, N. *Physica* **1949**, *15*, 386.
(28) Abragam, A. In *The Principles of Nuclear Magnetism*; Clarendon Press: Oxford, 1961.
(29) Carrington, A.; McLachlan, A. D. In *Introduction to Magnetic Resonance*; Harper & Row: New York, 1967.
(30) Shannon, R. D.; Prewitt, C. T. *Acta Crystallogr.* **1969**, *B25*, 925.
(31) Alvarez, L. J.; Sanz, J. F.; Capitan, M. J.; Odriozala, J. A. *Chem. Phys. Lett.* **1992**, *192*, 463.
(32) Kung, H. H. *Stud. Surf. Sci. Catal.* **1989**, *45*, 7.
(33) Weast, R. C., Ed. In *Handbook of Chemistry and Physics*, 52nd ed.; The Chemical Rubber Co.: Cleveland, OH, 1971−1972.
(34) Weckhuysen, B. M.; Schoonheydt, R. A. *Zeolites*, **1994**, *14*, 360.
(35) Weckhuysen, B. M.; Schoonheydt, R. A. *Stud. Surf. Sci. Catal.* **1994**, *84*, 965.
(36) Weckhuysen, B. M.; Spooren, H. J.; Schoonheydt, R. A. *Zeolites*, **1994**, *14*, 450.

JP9416432